Isospin and strong coupling effects in neutron scattering from even-A Se isotopes

J. Lachkar, M. T. McEllistrem,* G. Haouat, Y. Patin, J. Sigaud, and F. Coçu
Service de Physique Nucléaire, Centre d'Etudes de Bruyères-le-Châtel, B.P. No. 561, 92542 Montrouge, Cedex, France
(Received 1 December 1975)

Differential cross sections for elastic scattering from the even-A isotopes of Se have been measured at 6, 8, and 10 MeV. Inelastic scattering differential cross sections have been obtained at 6- and 8-MeV incident energies. The results have been analyzed in a coupled channel model to determine the isospin coefficients in the real and imaginary parts of the scattering potential and the deformation parameters β_2 appropriate to neutron scattering in these vibrational nuclei. Both the coupling to the first 2^+ level and the imaginary scattering potential vary strongly between ^{76}Se and ^{82}Se, and in such a way that their effects cancel each other for inelastic scattering. It is shown that with an adequate data set the strong coupling and isospin dependencies of neutron scattering can be separated. The normalization uncertainty of these measurements is about 7%, and the statistical precision ranges from 1 to 10%.

[NUCLEAR REACTIONS ^{76}Se, ^{82}Se(n,n) and (n,n'), E_n=6–8 and 10 MeV, ^{78}Se, ^{80}Se(n,n), and (n,n'), E_n=8 MeV. Measured (E_n,θ). Enriched targets. Coupled channel analysis.]

I. INTRODUCTION

The study of fast neutron scattering by the even-A isotopes of Se has enabled us to observe the effects of strong coupling between the first excited 2^+ level and the ground state in neutron scattering. For a proper interpretation of the differential scattering cross sections it has been necessary to separate the effects of coupling to the first 2^+ level from the effects of weak coupling to the many other excited levels. These latter effects are represented by the strength of the absorptive term in a complex potential description of the scattering cross sections, the usual means of representing all absorptive processes in fast neutron scattering. The large variation of the parameter $(N-Z)/A \equiv \xi$ for the different isotopes has enabled us to observe in addition the strong neutron excess dependence of the real and absorptive scattering potentials. The interrelation between strong coupling and neutron excess dependence is shown to be important.

Since this study is carried out within the framework of a complex potential analysis, the form of the potential $\bar{U}$ is presented here:

$$-\bar{U} \equiv Vf(r,a,R) + i\left[W_D 4a_s \frac{d}{dr} f(r,a_s,R_s) + W_V f(r,a_V,R_V)\right] + V_{ls}(\hbar/m_\pi c^2)\vec{\sigma}\cdot\vec{l}\frac{1}{r}\frac{d}{dr}[f(r,a_{ls},R_{ls})].$$

The form factor f is $f(r,a,R) = \{1+\exp[(r-R)/a]\}^{-1}$. Two types of potential analyses were performed, differentiated by the treatment of the radius. For a conventional one-channel analysis, the radius was $R = R_0 A^{1/3}$ fm, a single fixed radius for all terms of the potential. A second analysis coupled the 0^+ ground and 2^+ first excited levels explicitly, in a vibrational model of the scattering. For this the radius is written $R = R_0[1+\sum_\lambda \beta_\lambda Y_{\lambda 0}(\theta)]$ for the deformable terms V and W_D. The parameter β_2 determined the strength of the coupling. For the terms not deformed, W_V and V_s, $R = R_0 A^{1/3}$ fm. The constant $R_0 = 1.25$ was used throughout this work.

The potential strengths V and W_D are $V = V_0 - \alpha E - \xi V_1$ and $W_D = W_0 + \alpha_s E - \xi W_1$, where E is the incident energy, α and α_s are constant coefficients. It is the comparison of the neutron excess dependencies V_1 and W_1 for the two analyses which is the focus of this work, as well as the strength of the vibrational coupling in the second analysis.

The four even-A isotopes of Se were chosen for this study of fast neutron scattering for several reasons. Most importantly, they form a set of nuclei with very similar, apparently vibrational, level schemes. The low-lying levels of all of them seem to be one- and two-phonon multiplets, with the two-phonon triplets separated in energy from other excitations. The excitation energies of the one-phonon states vary no more than about 15% throughout these nuclei, as is shown in Fig. 1. In addition to the vibrational low-lying levels, there are other strong similarities between the level and decay schemes of the four isotopes, as revealed in a study[1] of the Se$(n,n'\gamma)$ reactions, a companion experiment of this one. The number of levels below 3.5-MeV excitation energy varies only from 24 to 27 for three of the nuclei and is

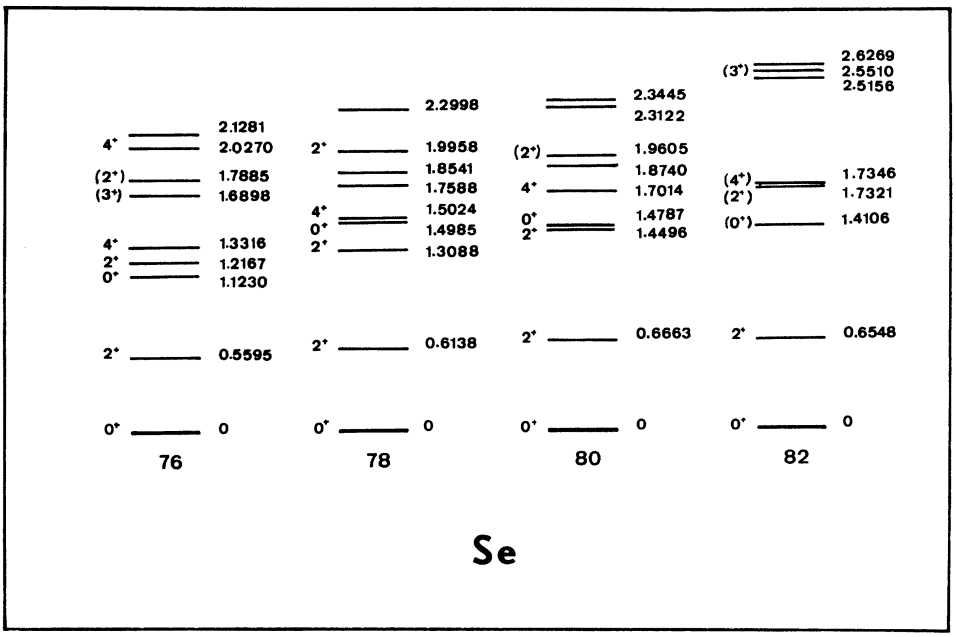

FIG. 1. Low-lying level schemes of the four even-A Se isotopes, showing the one- and two-phonon multiplets in each nucleus, and a few higher levels.

33 for the fourth, ^{78}Se.

There is, however, one property of these isotopes which varies in an unusual way from one isotope to the next; that is the deformation amplitude β_2 for the first excited 2^+ level. As determined from Coulomb excitation experiments,[2,3] and assuming a uniformly charged sphere of radius $r = 1.25A^{1/3}$ fm, the values range from $\beta_2 = 0.175$ for ^{82}Se to $\beta_2 = 0.28$ for ^{76}Se. They become progressively larger as one goes away from the closed neutron shell $N = 50$, and in any case they are inordinately large for a set of vibrational nuclei.

As on the whole the even-A Se nuclei appeared to be quite similar, and the neutron excess varied considerably for this set of isotopes, $\xi(82) - \xi(76) = 0.065$, the original concept of the experiment was to study the ξ dependence, viz., isospin dependence in neutron scattering. We expected that the small changes in real and absorptive potentials commonly ascribed[4,5] to the isospin dependence would be evident in this study. Extensive reviews of proton scattering[6,7] seem to define the coefficient V_1 of the ξ dependent term in the real potential to be between 24 and 27 MeV. The corresponding coefficient W_1 in the imaginary surface potential is much more difficult to determine, partly because proton inelastic scattering cross sections are not very large. Nonetheless, Becchetti and Greenlees[6] did propose in their analysis that $W_1/V_1 \sim \frac{1}{2}$. Later, an extensive study of "quasielastic" scattering to analog states in (p,n) reactions[8] seemed to suggest larger values for W_1, with $W_1 \sim V_1$ for protons. This analysis[8] is comprehensive because it combines analyses of proton scattering from the targets, neutron scattering from the residual nuclei, and form factor determinations to fit the magnitude of the (p,n) cross sections. The results are somewhat ambiguous, however, because some of the fits to neutron scattering data are rather poor, an unhappy result of all of the constraints imposed upon the potentials.

Attempts to determine the ξ dependence in neutron scattering are on the whole less conclusive, largely because of the lack of accurate measurements above an incident energy of 4 MeV. Below that energy, level-scheme differences seem to dominate the neutron scattering differences,[9] and it is unlikely that these can be ascribed directly either to the ξ dependence or to the isospin dependence, two dependencies which may or may not be the same. The most extensive higher energy survey, that of Holmquist and Wiedling[10] at 8 MeV, suggested a neutron-excess coefficient V_1 only half that obtained in proton scattering. Other experiments and analyses were reported[5] yielding coefficients as small or smaller than that of Holmquist and Wiedling. On the other hand, a very limited survey[11] of the Ni region at an incident energy of 9 MeV produced a coefficient $V_1 \simeq 22$ MeV, in good agreement with the one found for proton scattering. Confidence in this last result is

strengthened by the fact that the analysis also gave a good fit to asymmetries from polarized proton scattering from Co, one of the target nuclei of the neutron scattering experiment.

To our knowledge, definite statements about the ξ dependence of the absorptive potential in neutron scattering come only from the analysis of s-wave neutron strength functions by Newstead and Delaroche.[12] The data show two trends, a gradual increase in S_0 from element to element as A increases in the region $A \sim 90-140$, and a very sharp decrease within a set of isotopes as the neutron excess increases. The first trend implies a very small W_1, but the second requires[12] a very large W_1, with W_1/W_0 ratios ranging from 3 to 5.

The questions of interest in this study, then, were the effects of strong coupling to 2^+ levels, and the neutron excess dependence of the real and imaginary potentials used to describe the scattering. Incident energies of 6, 8, and 10 MeV were chosen for the measurements. These energies were deemed high enough to avoid difficulties of interpretation caused by small differences in low-lying level schemes and uncertainties associated with compound elastic contributions to the elastic scattering cross sections. They were low enough to permit measurements with good resolution within limited data-taking periods.

II. EXPERIMENTAL SYSTEMS AND PROCEDURES

A. Experimental system

A fast neutron scattering program is performed at the tandem accelerator laboratory of the Centre d'Etudes de Bruyères-le-Châtel. The characteristics of the neutron time-of-flight facility developed for these measurements have not been extensively presented before, and thus will be described in some detail in connection with this experiment. Future reports of experiments in this series should then require only brief descriptions of changes needed for particular measurements. The measurements are carried out in a thin-walled rectangular neutron "hall" 30 m × 50 m. The beam line enters parallel to the long axis of the hall but off center, to permit flight paths for neutron detection at least to 18 m at all angles between 0 and 160°. The beam extension terminates over the center of a cylindrical "pit" in the floor, which extends 3 m below floor level and has a radius of 5 m. The neutron source is mounted at the end of the extension, close to the center of the pit.[13]

Deuterons or protons accelerated in the 14-MeV tandem accelerator are obtained from a pulsed ion injector, operated at 120-kV preinjection voltage. The 120-keV ions are chopped and bunched into

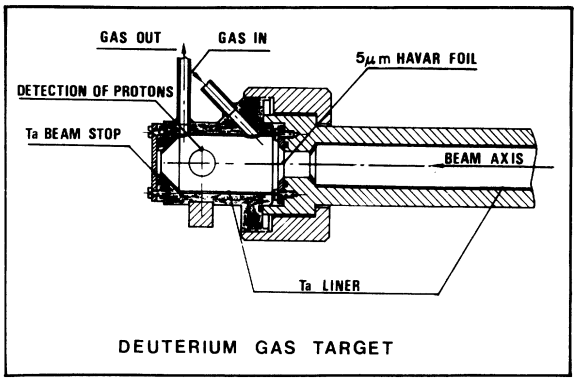

FIG. 2. Deuterium gas target cell and assembly.

bursts of repetition rate 2.5 MHz and width 1 ns full width at half maximum (FWHM). The average current is usually about 3 μA.[13] The beam terminates in either a deuterium or tritium gas cell, since neutrons are generally produced either from the ^{2}H$(d,n)^3$He or ^{3}H$(p,n)^3$He neutron source reactions. The deuterium gas cell is 3 cm long and at 1 atm pressure. The gas is isolated from the accelerator vacuum system by a 5-μm-thick Havar foil. To improve the cooling of the window, the deuterium gas is circulated through a cooling system and returned to the target cell through a small tube aimed at the window. Figure 2 shows the details of construction. The stainless-steel gas cell is lined with tantalum and has a beam stop, also in tantalum. This material was chosen to reduce unwanted neutrons from (d,n) reactions and also to minimize neutrons from drive-in targets formed at surfaces struck by the beam.

The tritium gas cell is a nickel cylinder, 3.0 cm in length, with a nickel entrance window having a thickness of 0.5×10^{-3} cm. As can be seen in Fig. 3, the cell is mounted behind a small chamber

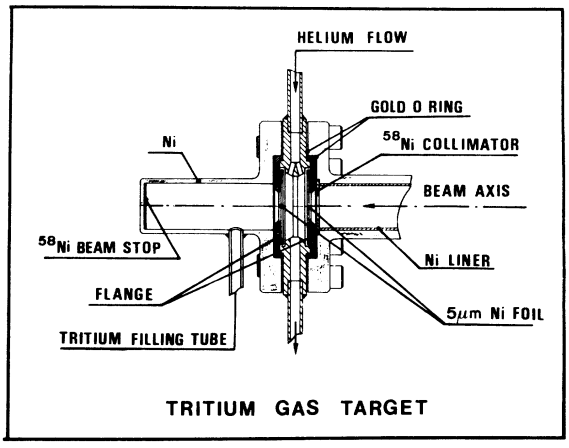

FIG. 3. Tritium gas target cell and assembly.

closed by a second nickel foil. Between these two foils, helium gas is circulated. With this arrangement safe- and long-duration experiments are carried out with currents as high as 4 μA with negligible tritium contamination in the accelerator extension.[14] The tritium cell was at 1.5 atm pressure for the present experiments. The beam stop is a disk made of ^{58}Ni, whose Q value for the (p,n) reaction is $Q = -9.35$ MeV.

Scattered neutrons are detected by an array of four detectors placed at 20° intervals. Each detector consisted of a 12.5-cm diam 5-cm thick NE-213 liquid scintillator optically coupled to an XP-1040 photomultiplier tube. The flight path was 8 m long for all incident energies. The shielding arrangement is presented in Fig. 4. Each detector was housed in a heavy shield of polyethylene and lead behind a 1.5-m long collimator of paraffin loaded with Li_2CO_3 and borax. Four 70-cm long iron shadow bars with tungsten tips reduced the background caused by direct neutrons coming from the source. For a multiple detector system such as this one the shadow bars must be further from the scattering sample than one would like them to be. Furthermore, it is extremely difficult to arrange them so that surfaces of the shadow bars illuminated by the source are well shielded from the detectors. To avoid shadow bar illumination by the source a separate Pb block was placed near the source, to shadow the tips of the 70-cm bars. The configuration, placement, and size of this block depended on the angular placement of the four-detector array. Additional intermediate collimators of paraffin + Li_2CO_3 were placed between the detector shielding and the 70-cm bars. The acceptance solid angle at the scatterer of the detectors was defined by an hourglass shaped-Cu baffle which was the lining of these intermediate collimators. A low concrete block wall shielded the detectors against neutrons scattered from the edge of the 5-m radius pit, and from the floor under the detectors.[13]

B. Electronic apparatus

The block diagram of the electronic apparatus is shown in Fig. 5. Pulse shape discrimination is used to reject most of the γ-ray induced events in the scintillators. For timing measurements fast

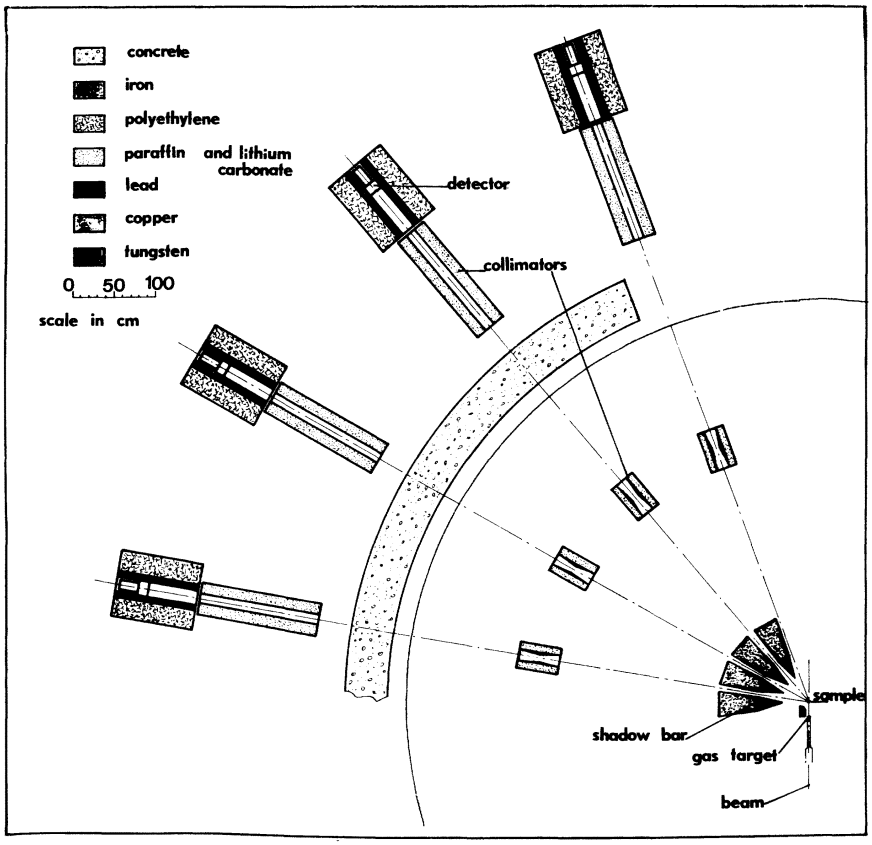

FIG. 4. The experimental arrangement used to measure the differential cross sections of the Se isotopes at 6–8 and 10 MeV neutron energies.

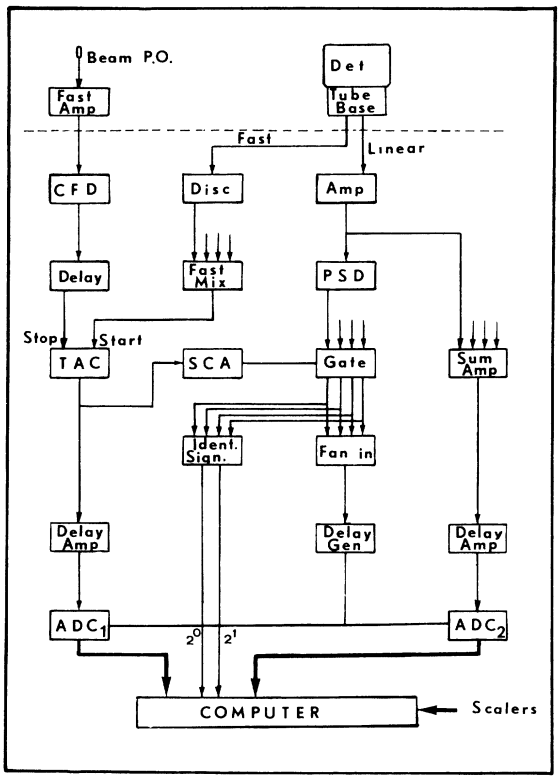

FIG. 5. Block diagram of the electronics used in the neutron time-of-flight spectrometer.

pulses from the anode of the four photomultipliers are mixed, after being properly shaped by constant fraction discriminators. They then enter a time-to-amplitude converter (TAC). Pulses from an inductive beam pick-off cylinder are used to stop the TAC. The output of the TAC is recorded in a two-parameter mode with the linear output of the photomultiplier. The identification of the detector, as a particular one of the four, is given by an auxiliary coincident pulse. The nominal electronic resolution is about 1 ns (FWHM), as checked by coincident measurements with ^{22}Na γ-ray sources.

C. Experimental procedure–Se measurements

Differential cross section measurements for selenium isotopes were made at 6-, 8-, and 10-MeV incident energies. Incident 8-MeV neutrons were produced from the ^{2}H$(d,n)^3$He reaction. The energy spread of the neutron beam due to straggling in the entrance foil, energy loss in the gas, time spread from target length, and finite size of the scattering sample was 300 keV. It was small enough to ensure good separation of the first excited level from the ground state for all the Se isotopes. At 6- and 10-MeV energies, the incident neutrons were produced from the ^{3}H$(p,n)^3$He reaction. The overall energy spreads were 180 and 150 keV, respectively. The largest contributions were from proton straggling in the windows and the energy loss in the target gas.

Each selenium sample was in the form of metallic powder with an isotopic enrichment greater than 90%. Their compositions are given in Table I; they were on loan from the USSR. Each of them was contained in a polyethylene can of diameter 25 mm and height 50 mm. The cell-to-sample distance was about 12 cm at 8-MeV neutron energy and 8.25 cm at 6- and 10-MeV energies. The sample was placed at 0° with respect to the incident beam.

Measurements were completed over the angular range from 20 to 150° at 16 angles for data taken at 6-MeV incident energy, 24 angles at 8 MeV, and 18 angles at 10 MeV. The smaller number of angles used at 6 and at 10 MeV was the consequence of limited availability of the separated isotope Se samples. Angular settings were determined with an accuracy of ±0.2°. For each set of four detector angles, runs were made with the Se powder samples in polyethylene containers and with the empty containers. The container runs were later subtracted from the Se sample runs. No correction for neutron attenuation was made for the empty container runs, since the attenuation was less than 6%, and the container yields were

TABLE I. Experimental conditions. Incident neutron energies are 6.00, 8.00, and 10.00 MeV; flight path is 8 m; sample is powdered metal; container is 25 mm × 50 mm, 1 mm thick wall (polyethylene); cell-to-sample distance is 12.25 cm at 8-MeV neutron energy, 8.25 cm at 6- and 10-MeV neutron energies.

Sample	Isotopic composition of the samples						Total mass of the sample (g)
	74	76	77	78	80	82	
^{76}Se	0.08	90.50	4.35	2.66	4.63	0.78	49.7
^{78}Se	0.02	0.48	0.40	97.90	1.32	0.18	40.7
^{80}Se	0.01	0.09	0.09	0.32	99.20	0.29	48.1
^{82}Se	0.06	0.62	0.56	4.76	4.80	92.20	43.6

small compared to the elastic Se yields whenever the two groups interfered with one another.

D. Monitoring and absolute flux measurement

The flux of incident neutrons is monitored simultaneously by several methods. Its measurement, though difficult, is extremely important if good accuracy is to be attained with confidence in the results. The integrated charge of the beam during each run is recorded. Also, a liquid scintillator (NE-213) with n-γ discrimination is used in the time-of-flight mode for monitoring the primary neutron beam. It views the target at 55° to the incident beam. In experiments using the ^{2}H$(d,n)^3$He reaction for neutron production, we count in addition the number of the protons produced by the ^{2}H$(d,p)^3$H reaction from the target gas. The protons are detected by two surface-barrier diodes facing each other and placed at 90° relative to the incident beam. They view the source through windows in the target holder. The proton and neutron monitoring systems were consistent with each other to within 0.3% during the Se experiment.

The neutron flux was determined using the n-p scattering cross section at 0° as a standard,[15] measured with an angular spread of ±6°. The measurement was done with a proton-recoil counter telescope whose efficiency was calculated analytically, taking into account the target and the detector geometries. This calculation agreed within 3% with experimental results obtained by the associated particle method for 2.5- and 14.1-MeV neutron energies. The overall accuracy in flux measurements was about 5%. The solid angle of the counter telescope during a telescope run was almost the same as that of the sample during a sample run.

The neutron-detector efficiency is required for the determination of the absolute differential cross sections. It was measured by two independent methods. In the first one, we counted directly monoenergetic neutrons from the target produced by the ^{2}H$(d,n)^3$He reaction.[16] In the second, an $(n$-$p)$ scattering experiment was performed using a polyethylene sample (1-cm diam by 4-cm height). These two measurements were found to be consistent within 5% when the former were corrected for deadtime in the counting electronics.

E. Data reduction, corrections and uncertainties

The data reduction process permitted off-line adjustment of the energy threshold for neutron detection. In these measurements, only scintillator pulses which correspond to neutron energies greater than 2.5 MeV at 6 and 8 MeV incident energies and 3.5 MeV at 10 MeV incident energy were used. The measurements at 6 and 8 MeV have also been reduced with a threshold set at 3.5 MeV; the deduced cross sections have been found to be consistent, within the statistical accuracy, with those using the threshold at 2.5 MeV. This agreement gives confidence in the background subtraction methods.

Yields in the peaks due to neutrons scattered by the Se samples were converted to differential cross sections. They were corrected for neutron flux attenuation in the sample, multiple scattering, and geometrical effects. To make these corrections an analytic method due to Kinney[17] and a Monte-Carlo method[18] were used. The corrected values from the two correction procedures were consistent within 3%, the largest differences occurring near sharp minima. Uncertainties in the measured cross sections due to finite-sample corrections were $\leq 2\%$. Other relative uncertainties arose from counting statistics and background subtraction. At most angles these uncertainties ranged from 1 to 5%, but at some angles, near 90°, neutrons elastically scattered by carbon had almost the same energy as those from inelastic scattering to the first excited level of the Se isotopes, and therefore they could not be resolved experimentally. At those angles, the uncertainties for the inelastic yields became as large as 15%. The absolute neutron detector efficiency was estimated to have an uncertainty of 5%. The above uncertainties, along with that of the neutron flux measurement already discussed, were quadratically added to give the experimental error. Absolute cross sections are given with an overall uncertainty varying between 7 and 20%.

III. RESULTS AND INTERPRETATION

A. Results

Differential scattering cross sections were measured at 6-MeV incident energy. The corresponding for the shape elastic scattering for both ^{76}Se and ^{82}Se are plotted together in Fig. 6. The inelastic scattering measurements are plotted separately in the lower panel of this figure. The compound elastic contributions have been estimated and will be discussed later. The curves are calculations that will be presented in Sec. III B. The essential results are directly evident in the data as follows: one notes that the elastic scattering cross sections for all angles beyond the forward peak show values for ^{76}Se lower than those for ^{82}Se by almost a common factor. A potential representation can reproduce such a difference only if the strengths of the absorptive potentials are markedly different for the two nuclei.

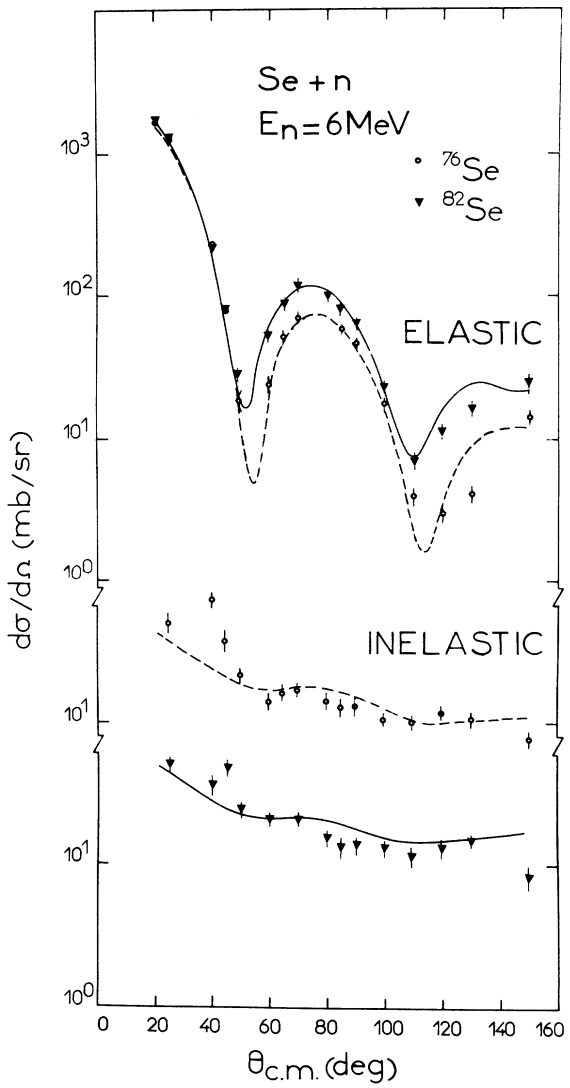

FIG. 6. Elastic and inelastic scattering cross sections at an incident energy 6 MeV for ^{76}Se and ^{82}Se. All curves are coupled channel calculations as described in the text.

On the other hand, the inelastic scattering cross sections are almost the same for both nuclei, in spite of the fact that one would expect them to differ by more than a factor of 2. The expectation is based on the fact that the β_2 values for the two nuclei are known to differ by 50%, and direct excitation of the states should be proportional to β_2^2. Thus, the near equality of the inelastic scattering cross sections requires an explanation. A suggestion would be that compound system processes are important, and they are completely insensitive to dynamical properties of the excited levels. Detailed calculations carried out in connection with our analyses show, however, that those processes could account for less than 10% of the measured yields.

The most complete set of data was obtained at an incident energy of 8 MeV, where elastic and inelastic scattering cross sections were obtained for all four Se isotopes. The results are presented in Figs. 7 and 8. The shape elastic scattering cross sections show the same behavior as observed at 6 MeV; that is, the values for all angles beyond the forward maximum are systematically lower as one goes from ^{82}Se to ^{76}Se. The progression is quite regular as one goes from isotope to isotope. This regular progression was pointed out when preliminary results for these elastic scattering cross sections were reported at the Conference on Nuclear Cross Sections and Technology.[12] The inelastic scattering cross sections to the strongly collective 2^+ states are also shown in Figs. 7 and 8, and the values are nearly the same for all four isotopes. If they were plotted together they would seem to produce a single angular distribution, this again in spite of the fact that the β_2^2 values are markedly different for all of the isotopes.

Elastic cross sections were also obtained for both ^{76}Se and ^{82}Se at 10 MeV incident neutron energy. The data are plotted in Fig. 9.

B. Interpretation

As mentioned above, it should be noted here that for the elastic scattering data the points plotted in Figs. 6, 7, and 8 are not the measured values themselves, but the measurements after estimates of the compound elastic scattering cross sections (CE) have been subtracted. The CE contributions were obtained from Wolfenstein-Hauser-Feshbach calculations[20] which included all known levels of the Se isotopes up to an excitation energy of 4.0 MeV. The failure to include levels above this energy was partially compensated by also neglecting the CE enhancement factors predicted by Satchler[21] and Moldauer[22] and found to be necessary in recent low energy experiments[23] where the CE contributions can be well extracted. The CE corrections to the data in the present experiment were small and essentially insignificant except at the minima in the elastic angular distributions. For data at 6 MeV they ranged from 3 mb/sr at large and small angles to 0.9 mb/sr near 90°, and at 8 MeV they were about one-half as large. They were found to be negligible at 10 MeV. As estimates of the compound nucleus contributions to the inelastic scattering to the first 2^+ states were found to be negligible at all energies, the corrections were not taken into account. Points on Figs. 6, 7, and 8, thus, show the experimentally measured values.

1. First analysis. Our first analysis effort was

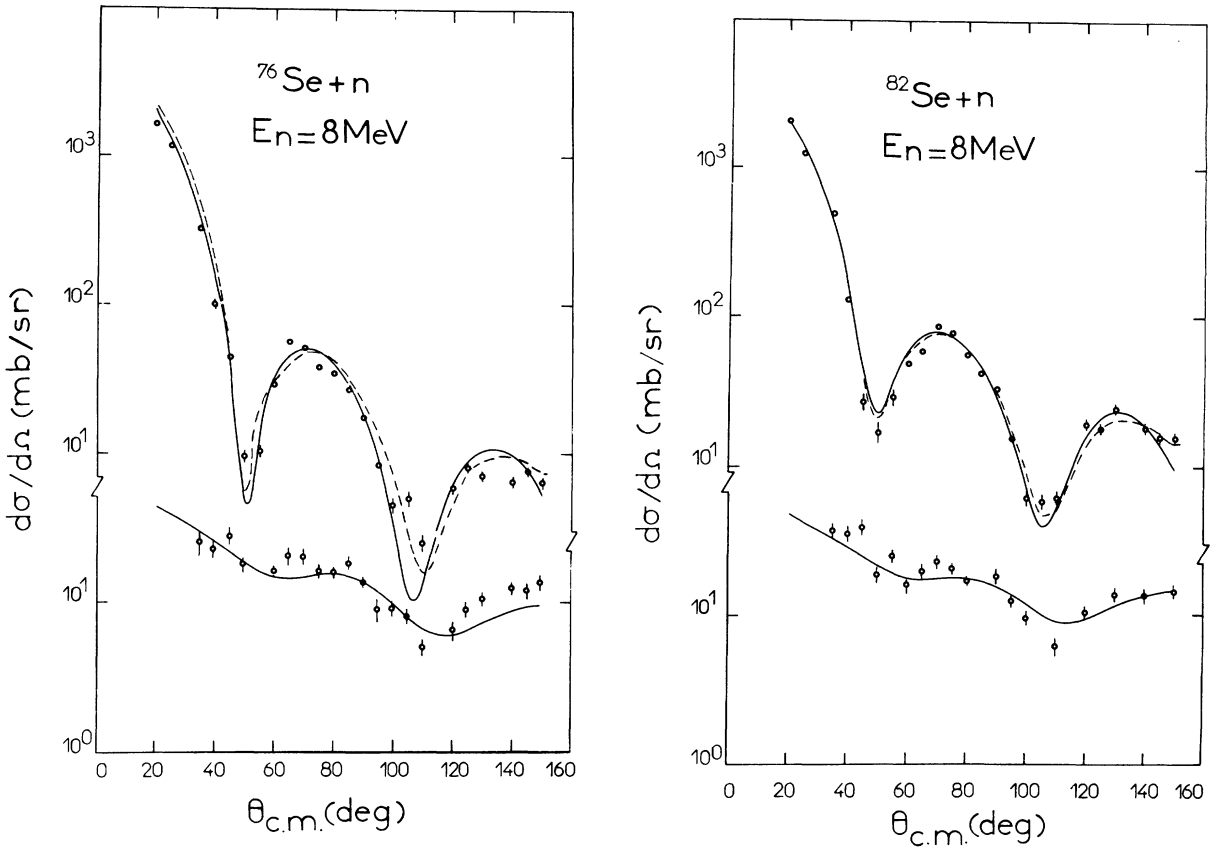

FIG. 7. Elastic and inelastic differential scattering cross sections for ^{76}Se and ^{82}Se at an incident energy of 8 MeV. The dashed curves for elastic scattering are the results of a one-channel spherical potential fit to elastic scattering only. The solid curves are coupled channel calculations.

concentrated on a conventional complex potential representation of the elastic scattering differential cross sections, and on a search for consistent potential parameters at the three incident energies. The description of that analysis was the object of a report to the Conference on Nuclear Cross Sections and Technology,[19] and only some of the results are presented here for the sake of the completeness of the present discussion. The reader is thus referred to the above report for a more detailed description of the parameter search made. The parameters of the potential found to fit the measurements at the three incident energies are given in Table II, and the corresponding fits with this single-channel model are shown in Figs. 7 and 8 as dashed curves. The fits are shown for the 8-MeV data because the most extensive set of data was obtained at that energy, and accordingly the most extensive search of parameters was made there.

We draw attention to the coefficient of ξ in the real potential $V = V_0 - \alpha E - \xi V_1$, with $V_1 = 9.3 \pm 1.8$ MeV, and in the absorptive surface potential $W_D = W_0 + \alpha_s E - \xi W_1$, with $W_0 = 13.7$ MeV and $W_1 = 43.2$ MeV. The coefficient V_1 is less than half that usually reported in proton scattering studies, where values ranging between 24 and 27 MeV are usually found.[7] The value found here of 9.3 ± 1.8 MeV is consistent with the value 13 ± 6 MeV reported by Holmquist and Wiedling in their survey of neutron scattering[10] at an incident neutron energy of 8 MeV, and with comparably small values suggested in a recent review of neutron scattering.[5] Thus, several neutron scattering analyses lead to coefficients V_1 too small to be consistent with those from proton scattering, if i-spin dependence is to relate neutron scattering potentials to those for protons. The coefficient W_1 in the absorptive potential is nicely consistent with those determined from earlier potential fits to s-wave strength functions within sets of isotopes. The value $W_1 = 45$ had been obtained in a fit to strength functions for the Sn isotopes, for example,[12] so that the reported strong neutron excess dependence of W_D within sets of isotopes is found also in the rather different set of measurements presented

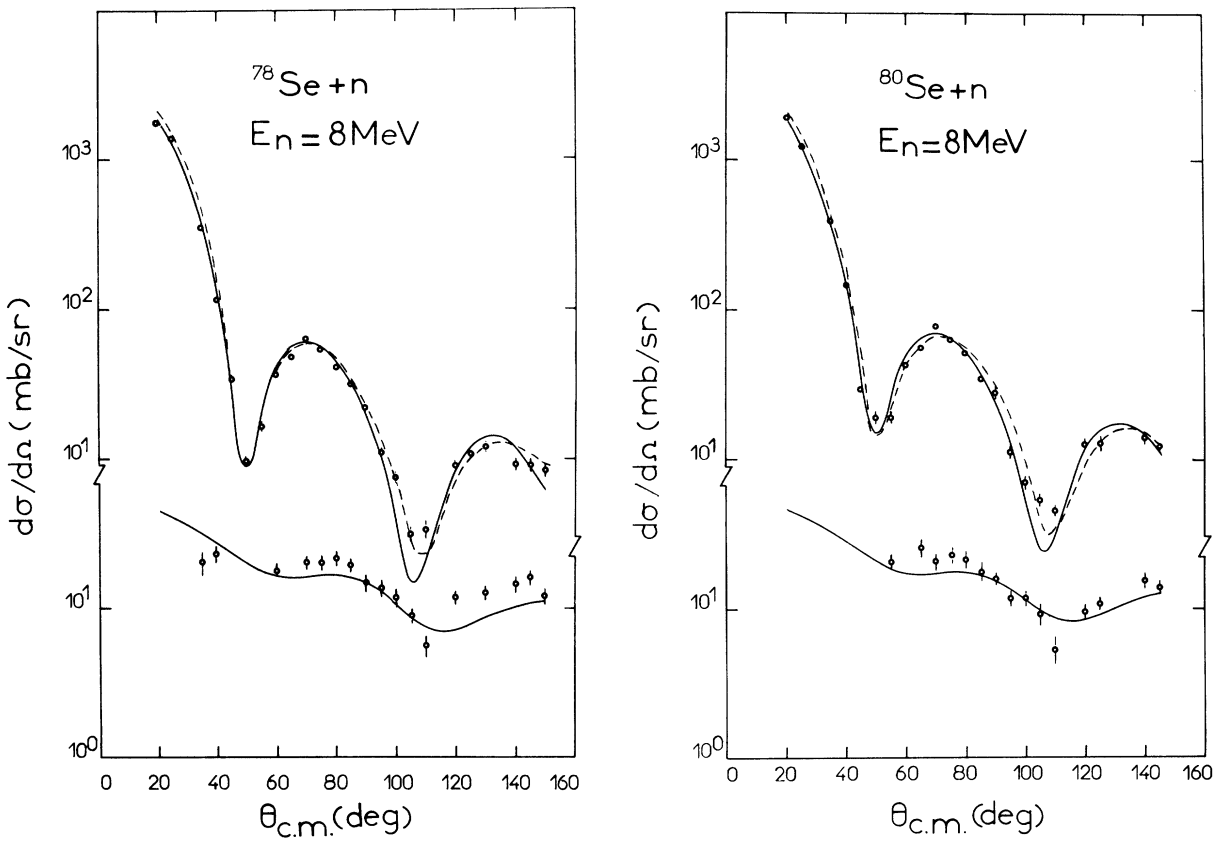

FIG. 8. Elastic and inelastic differential scattering cross sections for ^{78}Se and ^{80}Se at 8 MeV incident energy. The solid curves are coupled channel calculations made without any parameter adjustments after potentials were determined by fits to ^{76}Se and ^{82}Se data. The dashed curves are one-channel spherical potential fits to elastic scattering only.

here.

In order to describe the inelastic scattering cross sections, calculations were made in the distorted-wave Born approximation (DWBA) formalism using the potentials from the above elastic scattering analysis for the incoming and outgoing neutrons. Complex coupling derived from the scattering potentials was used as the form factor for the transition, and the calculations were made with the code DWUCK.[24] The results gave angular distributions consistent with the measurements, but the absolute magnitudes of the calculated cross sections were too low by almost an order of magnitude, when β_2 values from the Coulomb excitation experiments[2,3] were used.

In summary, the above one-channel analysis gave an explanation of the systematic differences between the elastic scattering cross section for the different isotopes as due to a large neutron excess dependence of the absorptive potential. The analysis treated the differences consistently for all the measurements. The surprisingly strong neutron excess dependence of W is consistent with a similar strong dependence noted by Newstead and Delaroche[12] in their explanation of the behavior of s-wave strength functions, but the large values of W required to fit the elastic scattering data resulted in DWBA calculations for the inelastic scattering cross sections which were much too small to fit the measurements. The inelastic scattering cross sections, 10 times as large as those expected on the basis of statistical model calculations, remained unexplained. Furthermore, the neutron excess dependence of the real part of the scattering potential is too weak to be consistent with the usual assumption of the isospin dependence in the scattering potential.

2. *Second analysis.* We turned next to an analysis in which the strong coupling of the ground and first excited states is explicitly taken into account. The coupled channel code JUPITOR[25] of Tamura was used for the calculations. The coupled channel method of analysis has been extensively developed by Lagrange[26] by including neutron data from a few

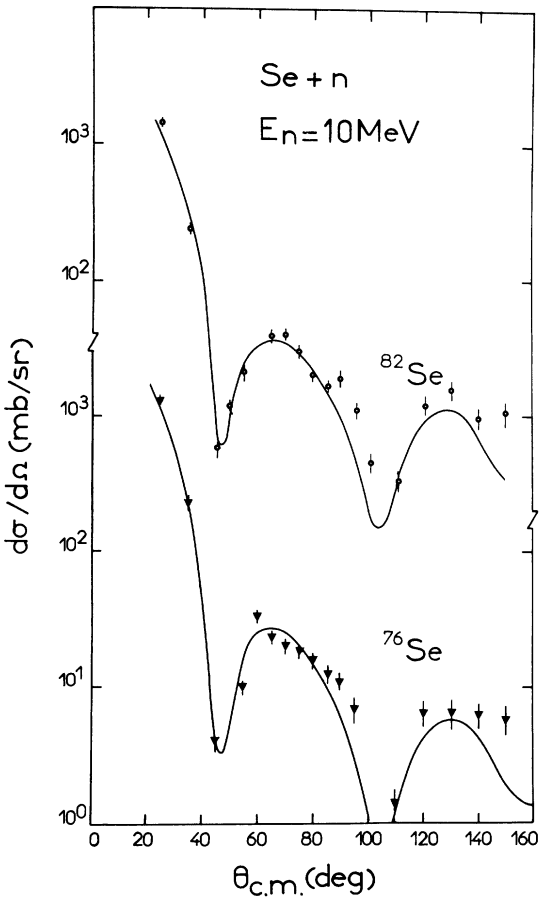

FIG. 9. Elastic scattering results for ^{76}Se and ^{82}Se at 10 MeV incident energy. The solid curves are results of coupled channel calculations.

keV to 20 MeV. The success of this method[26] encouraged us to include consideration of low energy neutron data in the present analysis.

Calculations were made by coupling the ground and first 2^+ states for each isotope. Some low energy properties thus obtained are listed in Table III for ^{76}Se, together with measured values when these exist.[27] The calculated s-wave strength function is probably a little too large, and the potential scattering radius R too small. This may mean that the potential as extrapolated to these low energies is too absorptive, but the values calculated are not far from those permitted by the measurements. Total cross sections calculated for several energies between 1 and 10 MeV are in excellent agreement with measured values, when the calculations take into account the isotopic abundances of natural Se.

First tests of this coupled channel model for the differential cross sections were made at 8 MeV incident energy and the test results are shown in Figs. 7 and 8. Also presented, as dashed curves, are the results of the single-channel analysis discussed above, in Sec. III B 1. For the three isotopes with $A = 78-82$, the coupled channel fits are superior to the one-channel results, and small changes are mainly apparent at angles beyond 100°.

The most impressive results of the calculations are that, with a single set of parameters, one can explain simultaneously the fact that the elastic cross sections decrease regularly at angles beyond the first maximum as one goes from ^{82}Se towards ^{76}Se, while the inelastic cross sections remain essentially constant from isotope to isotope. Both of these effects represent the interplay of the neutron dependence of W and the changing β_2. For the inelastic scattering cross section, the increase in W from ^{82}Se to ^{76}Se damps the effect of the coupling between the two levels generated by β_2, so that the increase in β_2 values is just canceled by the companion increase in the absorptive potential W. For the elastic scattering cross sections, the two parameters act in the same direction; that is, the increases in β_2 and W both transfer flux from the elastic channel to the inelastic ones and thus decrease the elastic cross sections. The effects are particularly evident in the Se isotopes because the β_2 values are large and vary strongly from one isotope to another, and the ξ dependence of W is also strong, as shown in the parameters of Table II.

The final points to be discussed in this analysis are the neutron excess dependence of the scattering potential and the choice of deformation parameters. The introduction of strong coupling to the first excited 2^+ level reduced drastically the W values needed to account for the absorption to other levels, but left W still strongly ξ dependent. In fact, the W reported in Table II for the coupled channel analysis is quite consistent with those needed for strength function analyses.[12] The coefficient V_1 in the real potential could not be significantly less than the quoted value $V_1 = 20$ MeV, even using other potential geometries; values of V_1 ranging from 20 to 24 MeV were found to satisfactorily represent most of the data. These values are quite consistent with the existing knowledge of the isospin dependence. The strong coupling to the first 2^+ levels enhances the anomalously small V_1 found in the single-channel analysis.

The β_2 values used in this analysis are given in Table III. The analysis was begun with values reported from Coulomb excitation[3] after correcting them for the different radii assumed in the two studies. Also, the parameter searches were initially carried out for ^{76}Se and ^{82}Se only. For ^{76}Se the adopted β_2 is essentially the starting value.

TABLE II. Potential parameters used in this study. Parameters which have been adopted without any adjustment are labeled (A); those which have been optimized by χ^2 fitting to the data are labeled (O). Real potential is Saxon-Woods shape; surface imaginary and spin-orbit potentials are Saxon-Woods derivative shapes; volume imaginary potential is Saxon-Woods shape. The real parameters are denoted without any subscript, the surface absorption one with an s, the spin-orbit ones with ls, and the volume absorption one with V.

	Optical model calculation		Coupled channel calculations (with complex coupling term)	
Radii	$R=R_s=R_V=R_{ls}=R_0A^{1/3}$fm			
R_0 (fm)	1.25	(A)	1.25	(A)
Diffusivenesses				
a (fm)	0.67	(A)	0.66	(O)
a_s (fm)	0.60	(O)	0.56	(O)
a_{ls} (fm)	$=a$	(A)	$=a_s$	(A)
a_V (fm)	$=a$ (10 MeV only)	(A)	$=a_s$ (10 MeV only)	(A)
Real potential depth	$V=V_0-\alpha E-\xi V_1$			
V_0 (MeV)	49.0 ± 1.0	(O)	52	(O)
α	$0.32^{+0.02}_{-0.05}$ Deduced from all the data		0.35 Deduced from 6- and 8-MeV data	
V_1 (MeV)	9.3 ± 1.8	(O)	20	(O)
Absorption potential depth	$W_D=W_0+\alpha_sE-\xi W_1$			
W_0 (MeV)	13.7	(O)	9	(O)
α_s	$0.02\gtrsim0$	(O)	0.25	(O)
W_1 (MeV)	43.2	(O)	38.2	(O)
W_1/W_0	3.2	(O)	4.2	(O)
W_V (MeV)	0.95 (10 MeV only)	(O)	2 (10 MeV only)	(O)
Spin-orbit potential depth				
V_{ls} (MeV)	6.0	(A)	6.0	(A)

For ^{82}Se it quickly became apparent that larger values than those implied by Coulomb excitation results would be necessary, otherwise simultaneous fits to elastic and inelastic scattering would be impossible. The β_2 values employed in the coupled channel calculations shown in Fig. 6, at an incident energy of 6 MeV, were about 6% larger than those shown for calculations at 8 MeV. The parameters cannot be fixed with greater certainty than this, because accurate total cross sections are not available for the separate isotopes. Variations of β_2 of about 5% make barely noticeable alterations for the elastic scattering cross sections, and alter the inelastic results about 10%. This is within the experimental uncertainties of those measurements. The parameters tabulated in Table III are averages of 6-MeV and 8-MeV β_2 values for ^{76}Se and ^{82}Se, and the results from the 8-MeV analysis for ^{78}Se and ^{80}Se.

The potential parameters of the present analysis were extrapolated to 10-MeV incident energy, where once again realistic values were obtained from the total cross sections.[27] The elastic scattering data and the corresponding fits (full curves)

TABLE III. Calculated (present work) and experimental (Ref. 28) s-wave strength functions and scattering radius for ^{76}Se. Comparison of deformation parameters β_2 derived from Coulomb excitation (C. E.) experiments (Refs. 2, 3) and this experiment. The C. E. results are corrected to a radius of $1.25A^{1/3}$ fm.

	Low energy properties		Deformation parameters		
^{76}Se	Calculated	Experimental	A	(C.E.)β_2	$(n,n')\beta_2$
S_0	3.6×10^{-4}	$(1.7\pm0.7)\times10^{-4}$	76	0.28	0.28
			78	0.24	0.27
R'	6.2 fm	$\simeq6.8\pm0.2$ fm	80	0.21	0.25
			82	0.17	0.22

are shown for ^{76}Se and ^{82}Se in Fig. 9. One modification was required here from the trends indicated at other energies: the surface absorptive potential W_D would not suffice. To properly fit magnitudes at the broad maxima near 45 and 130°, it was necessary to have both surface and volume (W_V) components, as indicated in Table II.

In the present study, the analysis of most transitions to collective states treat the intensities in terms of the shape parameters of the scattering field, the "deformation parameters" β_2. Very recently Madsen, Brown, and Anderson[28] pointed out that, when the contributions of valence neutrons and protons to the transition intensities are substantially different, the intensity-determining parameters β_2 may require a different interpretation, since they would be ξ dependent. Such β_2 variations would be pronounced when either neutron-magic or proton-magic nuclei are studied; thus it becomes interesting to compare β_2 values determined from nucleon scattering to those determined from Coulomb excitation measurements.[28] The extraction of these parameters from nucleon scattering data for such detailed comparisons must be treated with great care, however, because the scattering field is also strongly dependent on the neutron excess ξ. As has been pointed out by Lagrange[26] and observed in the present analysis, there is a strong $W\beta_2$ ambiguity in the inelastic scattering cross sections. Fortunately, changes in β_2 act mainly for inelastic scattering, and the elastic scattering cross sections are sensitive to small changes in W. Hence simultaneous fits to elastic and inelastic scattering can resolve this ambiguity. To ascertain the ξ dependence of W one needs neutron and proton scattering from the same target, or else scattering from a set of isotopes, as in the present experiment.

Using the above procedure, we determined that acceptable fits to our data at 6-, 8-, and 10-MeV incident neutron energies fixed β_2 values to be slightly different than those inferred from Coulomb excitation experiments, about 16–20% larger for ^{80}Se and ^{82}Se. The departures noted are significant; moreover, they are in the expected direction, if one acknowledges that the incident neutrons will interact most strongly with protons, as discussed by Madsen *et al.*[28]

IV. SUMMARY

Differential cross sections for elastic and inelastic scattering to the strongly coupled 2^+ states have been measured for the even-A isotopes of Se at several incident energies. A conventional optical model analysis of the elastic scattering cross sections yielded a neutron excess dependent term in the real potential anomalously low compared to that found for proton scattering, a result also reported in some earlier neutron scattering surveys. A larger neutron excess dependent term in the real potential was found when an analysis was carried out in which the 2^+ states were explicitly coupled to the ground states, and thus the second analysis yielded results consistent with the existing notion of an isospin dependent scattering potential. The need to consider coupling explicitly for neutron scattering and possibly not for proton scattering undoubtedly stems from the large neutron inelastic scattering cross sections to collective states.

The analysis thus sheds more light on the problem of the isospin dependence in neutron elastic scattering and also provides a good description of the inelastic scattering. Small departures of the deformation parameters employed in this analysis from Coulomb excitation values for ^{80}Se and ^{82}Se may reflect shell effects as one approaches the neutron-magic ^{84}Se.

ACKNOWLEDGMENTS

A special debt of gratitude is owed to Mme. Beuve, whose generous and expert cooperation was essential to the rapid completion of the coupled channel calculations and to the efficient deployment of codes for that purpose. It is a pleasure also to acknowledge many informative discussions about reasonable potentials for these nuclei with Dr. J. P. Delaroche, who also performed several calculations to test parameters used in this analysis. Useful critical comments from Dr. N. Cindro have been received with great interest.

One of us (M. T. M.) wishes to acknowledge the privilege and pleasure of his association with the Centre d'Etudes de Bruyères-le-Châtel. We wish to acknowledge also the continued support and encouragement of Dr. André Michaudon in the pursuit of these studies.

*Present address: University of Kentucky, Lexington, Kentucky.

[1]J. Sigaud, Y. Patin, M. T. McEllistrem, G. Haouat, and J. Lachkar, in *Proceedings of the Conference on Nuclear Cross Sections and Technology, Washington, D. C., March 3–7, 1975* (National Bureau of Standards, Washington, D. C., 1975), Special Publication No. 425, Vol. II, p. 893.

[2]P. H. Stelson and F. K. McGowan, Nucl. Phys. 32, 652 (1962); P. H. Stelson and L. Grodzins, Nucl. Data A1,

21 (1965).
[3]J. Barrette, M. Barrette, G. Lamoureux, S. Monaro, and S. Marzika, Nucl. Phys. A235, 154 (1974).
[4]G. R. Satchler, in *Isospin in Nuclear Physics*, edited by D. H. Wilkinson, (North-Holland, Amsterdam, 1969), p. 389.
[5]G. R. Satchler and F. G. Perey, *Nuclear Structure Study with Neutrons* (Plenum, New York, 1974), p. 133.
[6]F. D. Becchetti and G. W. Greenlees, Phys. Rev. 182, 1190 (1969).
[7]F. G. Perey, Phys. Rev. 131, 745 (1963); C. M. Perey and F. G. Perey, At. Data and Nucl. Data Tables 13, 293 (1974).
[8]J. D. Carlson, D. A. Lind, and C. D. Zafiratos, Phys. Rev. Lett. 30, 99 (1973).
[9]A. B. Smith, P. Guenther, and J. F. Whalen, Nucl. Phys. A244, 213 (1975).
[10]B. Holmquist and T. Wiedling, Nucl. Phys. A188, 24 (1972); Phys. Lett. 26B, 620 (1972).
[11]D. E. Velkley, D. W. Glasgow, J. D. Brandenberger, M. T. McEllistrem, J. C. Manthuruthil, and C. P. Poirier, Phys. Rev. C 9, 2181 (1974).
[12]C. M. Newstead and J. P. Delaroche, *Nuclear Structure Study with Neutrons* (Plenum, New York, 1974), p. 142.
[13]A. Adam and J. Cabé, Nucl. Instrum. Methods 121, 339 (1974).
[14]G. Haouat and S. Seguin, Report No. CEA-N-1739, 1974 (unpublished).
[15]J. C. Hopkins and G. Breit, Nucl. Data A9, 137 (1971).
[16]R. L. Schulte, M. Cosack, A. W. Obst, and J. L. Weil, Nucl. Phys. A192, 609 (1972).
[17]W. E. Kinney, Nucl. Instrum. Methods 83, 15 (1970).
[18]R. E. Textor and V. V. Verbinski, Report No. ORNL 4160, 1968 (unpublished). A special Monte-Carlo code has been developed and used in this laboratory, and found to yield sample-size corrections to neutron scattering in good agreement with those of Ref. 11, and with the approximate methods of Ref. 17 [G. Haouat and M. Forge (unpublished)].
[19]J. Lachkar, G. Haouat, M. T. McEllistrem, Y. Patin, J. Sigaud, and F. Cocu, in *Proceedings of the Conference on Nuclear Cross Sections and Technology, March 3–7, 1975* (see Ref. 1), Vol. II, p. 897.
[20]L. Wolfenstein, Phys. Rev. 82, 690 (1951); W. Hauser and H. Feshbach, *ibid.* 87, 366 (1952); E. Sheldon and D. M. Van Patter, Rev. Mod. Phys. 38, 143 (1966).
[21]G. R. Satchler, Phys. Lett. 7, 55 (1963).
[22]P. A. Moldauer, Phys. Rev 123, 968 (1961); 129, 754 (1963); Rev. Mod. Phys. 36, 1079 (1964).
[23]P. Lambropoulos, P. Guenther, A. Smith, and J. Whalen, Nucl. Phys. A201, 1 (1973); F. D. McDaniel, J. D. Brandenberger, G. P. Glasgow, and A. G. Leighton, Phys. Rev. C 10, 1087 (1974).
[24]P. D. Kunz, University of Colorado (unpublished).
[25]T. Tamura, Rev Mod. Phys. 37, 679 (1965); Report No. ORNL-4152, 1967 (unpublished).
[26]C. Lagrange, (Paris) J. Phys. Lett. 35, 111 (1974); EANDC Topical Discussion, Tokyo, 1974 (unpublished).
[27]K. K. Seth, Nucl. Data A2, 299 (1966); *Resonance Parameters*, compiled by S. F. Mughabghab and D. I. Garber, Brookhaven National Laboratory Report No. BNL-325 (National Technical Information Service, Virginia, 1973), 3rd. ed., Vol. I, p. 34-2.
[28]V. A. Madsen, V. R. Brown, and J. D. Anderson, Phys. Rev. Lett. 34, 1938 (1975).